2006 PROCEEDINGS

"HOME ON THE RANGE"

AMTA

AUSTIN TEXAS

Oct. 22-27 2006

REDUCTION OF TRUNCATION ERROR IN THE NEAR-FIELD–FAR-FIELD TRANSFORMATION WITH PLANAR SPIRAL SCANNING

F. D'Agostino (1), F. Ferrara (1), C. Gennarelli (1), R. Guerriero (1), G. Riccio (1), C. Rizzo (2)

(1) D.I.I.I.E. – University of Salerno, via Ponte Don Melillo, 84084 Fisciano (SA), Italy.
(2) MI Technologies Europe, 3 Hither Green, Southbourne Emsworth, PO10 8JA, UK.

ABSTRACT

An elaborate and effective strategy for estimating the samples external to the measurement region in the planar spiral scanning is developed in this paper. It relies on the nonredundant sampling representations of the electromagnetic field and on the optimal sampling interpolation expansions of central type and uses the singular value decomposition method for extrapolating the outside samples. It is so possible to reduce the inevitable truncation error affecting the near-field reconstruction, thus giving rise to a more accurate far-field prediction. Numerical examples assess the effectiveness of the proposed technique.

Keywords: Extrapolation, Planar spiral scan, NF–FF transformations, Nonredundant representations of electromagnetic fields, Truncation error reduction.

1. Introduction

Each member of the antenna measurement techniques community can profit today by about fifty years of research activity on near-field data acquisition and related near-field to far-field (NF–FF) transformations. Over these years, many solutions have been proposed to meet the demands of the various applications [1, 2]. The measured NF data are usually transformed into FF patterns by using an expansion of the antenna field in terms of modes, i.e., a complete set of solutions of the vector wave equation in the region outside the source. Plane, cylindrical or spherical waves are generally used for representing the field, thus determining the geometry of the NF scanning surface. Each of the NF–FF transformation techniques has its own particular advantages and disadvantages depending on the type of radiating structure under consideration and the measurement requirements. Among the NF–FF transformation techniques, those employing the planar scannings are particularly suitable for high gain antennas radiating pencil beam patterns well within the solid angle specified by the edges of the antenna under test (AUT) and those of the scanning area.

As suggested by Rahmat-Samii et alii in [3], the complexity and cost of the measurement set-up, as well as the time needed for data acquisition, can be reduced by means of continuous and synchronized movements of the positioning systems of the probe and of the AUT. In order to satisfy these requirements, NF–FF transformation techniques using innovative spiral scannings [4] have been recently developed. In particular, an effective NF–FF transformation using a planar spiral arrangement of samples has been proposed in [5]. To this end, a nonredundant representation of the voltage data acquired by the measurement probe on the spiral has been developed by applying the theoretical results on the nonredundant sampling representations of electromagnetic (EM) fields [6]. Then, the choice of the spiral step equal to the sample spacing needed to interpolate the data along a radial line allows one to obtain the required two-dimensional optimal sampling interpolation (OSI) formula. It is so possible to reconstruct the NF data needed by the classical probe compensated NF–FF transformation with plane-rectangular scanning [7].

However, since the measurement region is always finite, an inevitable truncation error affects the NF reconstruction in the zone close to the boundary of such a region. As a consequence, the NF recovery results to be accurate in a zone smaller than the measurement one and this implies a decrease of the angular region wherein an accurate FF reconstruction is attained. Accordingly, to obtain an accurate field reconstruction in the whole measurement region, it becomes very important to estimate a proper number of samples external to it.

The goal of this paper is just the estimation of these outside samples, otherwise equal to zero in the application of the OSI algorithm. Such an estimation allows one to reduce the truncation error, thus giving rise to a more accurate FF reconstruction, also in the far out side lobe region. The extrapolation process relies on the knowledge of extra data acquired on very few peripheral rings and makes use of the singular value decomposition (SVD) algorithm [8] for determining the outside data.

2. Efficient sampling representation of the probe voltage

Let us consider the field radiated by an antenna and observed on a spiral lying on a plane located at distance d from AUT the center. Since the voltage V measured by a non directive probe has the same effective spatial bandwidth of the field, the theoretical results relevant to the nonredundant representation of EM fields [6] can be applied to such a voltage. Accordingly, if the AUT is enclosed in a sphere of radius a and the planar spiral is described by an analytical parameterization $\underline{r} = \underline{r}(\xi)$, it is possible to consider the probe "reduced voltage"

$$\tilde{V}(\xi) = V(\xi)\, \mathrm{e}^{\mathrm{j}\gamma(\xi)} \tag{1}$$

where $\gamma(\xi)$ is a phase function to be determined. The error, occurring when $\tilde{V}$ is approximated by a band-limited function, becomes negligible as the bandwidth exceeds a critical value W_ξ [6]. Therefore, such an error can be controlled by choosing a bandwidth equal to $\chi' W_\xi$, $\chi' > 1$ being an excess bandwidth factor.

According to the theoretical results in [6], a non-redundant sampling representation of the voltage on a planar spiral with constant angular step $\Delta\theta$ (see Fig. 1) can be developed by properly using the following expressions for the optimal phase function and parameterization:

$$\gamma(s) = \frac{\beta}{2} \int_0^s \left[\max_{\underline{r}'} \hat{R}\cdot\hat{t} + \min_{\underline{r}'} \hat{R}\cdot\hat{t} \right] \mathrm{d}s \tag{2}$$

$$\xi = \xi(s) = \frac{\beta}{2W_\xi} \int_0^s \left[\max_{\underline{r}'} \hat{R}\cdot\hat{t} - \min_{\underline{r}'} \hat{R}\cdot\hat{t} \right] \mathrm{d}s \tag{3}$$

where $\underline{r}'$ denotes the source point, s is the curvilinear abscissa along the spiral, $\hat{t}$ is the unit vector tangent to it at the observation point P, β is the wavenumber and $\hat{R}$ is the unit vector from the source point to P.

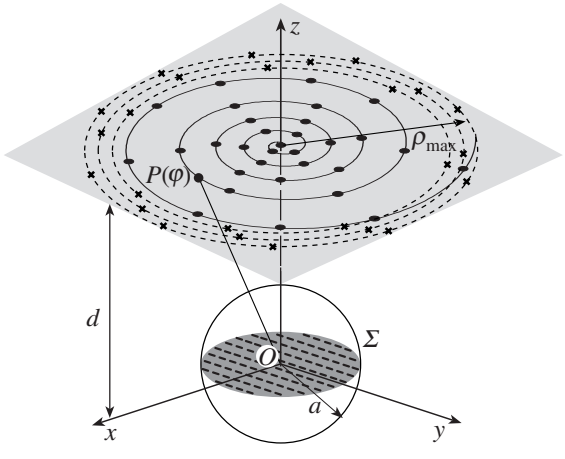

Figure 1 - Planar spiral scanning

The coordinates of P are given by:

$$\begin{cases} x = d\,\tan\vartheta\,\cos\varphi = \rho\,\cos\varphi \\ y = d\,\tan\vartheta\,\sin\varphi = \rho\,\sin\varphi \\ z = d \end{cases} \tag{4}$$

wherein φ is the angular parameter describing the spiral. It is worthy to note that the spiral angle $\vartheta = k\varphi$, unlike the zenithal angle θ, can assume negative values. Moreover, the spiral angle φ is always continuos, whereas, according to (4), the azimuthal angle ϕ exhibits a discontinuity jump of π when the spiral crosses the pole. Such a spiral can be obtained as intersection of the plane $z = d$ with the line from the origin to the point which moves on a spiral wrapping a sphere of unit radius. In order to allow the two-dimensional interpolation, the angular step $\Delta\theta$ of the spiral is chosen equal to the sample spacing required to interpolate the reduced voltage along a radial line. Then, the parameter k is such that $\Delta\theta$, fixed by two consecutive intersections $P(\varphi)$ and $P(\varphi + 2\pi)$ of the spiral with the consider radial line, is $\Delta\theta = 2\pi/(2M+1)$, with $M = \mathrm{Int}[\chi M'] + 1$ and $M' = \mathrm{Int}[\chi' \beta a] + 1$. Accordingly, being $\Delta\theta = 2\pi k$, it follows that $k = 1/(2M+1)$. The function $\mathrm{Int}[x]$ gives the integer part of x and $\chi > 1$ is an oversampling factor.

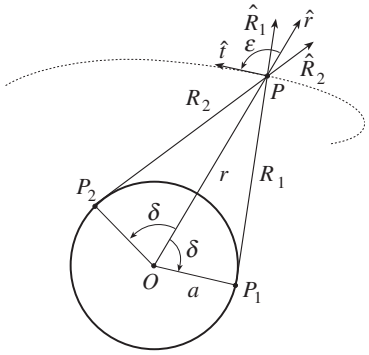

Figure 2 - Geometry in the plane $\hat{r}$, $\hat{t}$

It can be verified that the extreme values of $\hat{R}\cdot\hat{t}$ in (2) and (3) are determined by considering the intersection of the plane defined by $\hat{t}$ and the unit vector $\hat{r}$ (pointing from the origin to P) with the cone with the vertex at P and the generatrices coincident with the tangents to the AUT ball (see Fig. 2). As shown in [5] for the planar spiral, and in [4] with reference to the more general case of a spiral wrapping a quite arbitrary rotational surface, it results:

$$\gamma = \beta \int_0^r \sqrt{1 - a^2/r^2}\, \mathrm{d}r = \beta\sqrt{r^2 - a^2} - \beta a\, \cos^{-1}\left(\frac{a}{r}\right) \tag{5}$$

$$\xi = \frac{\beta a}{W_\xi} \int_0^\varphi \sqrt{k^2 + \sin^2 k\varphi'}\; \mathrm{d}\varphi' \tag{6}$$

Namely, ξ is proportional to the arclength of the spiral wrapping the sphere of unit radius. Since such a spiral is a closed curve, it is convenient to choose the bandwidth W_ξ such that ξ covers a 2π range when the whole curve on the sphere is drawn. Therefore,

$$W_\xi = \frac{\beta a}{\pi} \int_0^{(2M+1)\pi} \sqrt{k^2 + \sin^2 k\varphi'}\, \mathrm{d}\varphi' \tag{7}$$

According to these results, the OSI formula of central type [6] to reconstruct the field at any point of the spiral is:

$$\tilde{V}(\xi) = \sum_{n=n_0-q+1}^{n_0+q} \tilde{V}(\xi_n)\, \Omega_{N''}(\xi - \xi_n)\, D_N(\xi - \xi_n) \tag{8}$$

where $n_0 = \mathrm{Int}\big((\xi - \xi(\varphi_i))/\Delta\xi\big)$ is the index of the sample nearest, on the left, to the output point, $2q$ is the number of retained samples, and

$$\xi_n = \xi(\varphi_i) + n\Delta\xi = \xi(\varphi_i) + 2\pi n/(2N+1) \tag{9}$$

$$N = \mathrm{Int}(\chi N') + 1 \; ; \qquad N' = \mathrm{Int}(\chi' W_\xi) + 1 \tag{10}$$

Moreover,

$$D_N(\xi) = \frac{\sin\big((2N+1)\xi/2\big)}{(2N+1)\,\sin\big(\xi/2\big)} \tag{11}$$

$$\Omega_{N''}(\xi) = \frac{T_{N''}\Big[2\big(\cos(\xi/2)/\cos(\xi_0/2)\big)^2 - 1\Big]}{T_{N''}\Big[2/\cos^2(\xi_0/2) - 1\Big]} \tag{12}$$

are the Dirichlet and Tschebyscheff Sampling functions, $T_{N''}(\cdot)$ being the Tschebyscheff polynomial of degree $N'' = N - N'$ and $\xi_0 = q\Delta\xi$.

The OSI formula (8) allows one to evaluate the voltage at any point P on the scanning plane. As a matter of fact, it can be used for the evaluation of the "intermediate" samples, namely the voltage values at the intersection points of the spiral with the radial line passing through P. Once these samples have been determined, due to the particular choice of $\Delta\theta$, the voltage at P can be recovered by means of the following OSI expansion:

$$\tilde{V}(\theta,\phi) = \sum_{m=m_0-p+1}^{m_0+p} \tilde{V}(\theta_m)\, D_M(\theta - \theta_m)\, \Omega_{M''}(\theta - \theta_m) \tag{13}$$

where $m_0 = \mathrm{Int}[(\theta - \theta_0)/\Delta\theta]$

$$\theta_m = m\Delta\theta + k\phi = m\Delta\theta + \theta_0(\phi) \; ; \quad M'' = M - M' \tag{14}$$

$\tilde{V}(\theta_m)$ are the intermediate samples, and the other symbols have the same meaning as in (8).

3. Extrapolation procedure

Due to the finite sizes of the measurement plane, the reconstruction of voltage data is affected by an inevitable error in the zone close to the periphery of the scanning region. This will reflect in a decrease of the angular region wherein an accurate FF recovery is attained. In order to overcome this drawback, we now tackle the problem of estimating the voltage samples external to the scanning region $\rho \le \rho_{\max}$ on the measurement plane (see Fig. 1). To this end, let us assume, besides the regular samples acquired via the spiral scanning, the knowledge of the voltage data on the J rings spaced at a fixed step $\Delta\rho$, from the end of the measurement circle. On each of these rings, the extra samples are known at the points specified by

$$\phi_{n,j} = n\Delta\phi_j = 2n\pi/(2N_j + 1) \tag{15}$$

where

$$N_j = \mathrm{Int}(\chi N_j') + 1 \; ; \qquad N_j' = \mathrm{Int}(\chi^* W_{\phi_j}) + 1 \tag{16}$$

$$W_{\phi_j} = W_\phi(\theta_j) = \beta a \sin\theta_j \tag{17}$$

$$\chi^* = 1 + (\chi' - 1)\big[\sin\theta_j\big]^{-2/3} \tag{18}$$

$$\theta_j = \tan^{-1}\big[(\rho_{\max} - (j-1)\Delta\rho)/d\big] \quad j = 1,\ldots,J \tag{19}$$

On each radial line fixed by ϕ, the reduced voltage at the intersection points $P(\theta_j, \phi)$ with the extra rings can be evaluated via the OSI expansion [6]

$$\tilde{V}\big(\theta_j\big) = \tilde{V}\big(\theta_j, \phi\big) = \\ = \sum_{n=n_0-q+1}^{n_0+q} \tilde{V}\big(\theta_j, \phi_{n,j}\big)\, \Omega_{N_j''}\big(\phi - \phi_{n,j}\big)\, D_{N_j}\big(\phi - \phi_{n,j}\big) \tag{20}$$

where $2q$ is the number of retained samples along ϕ, $n_0 = \mathrm{Int}(\phi/\Delta\phi_j)$, and $N_j'' = N_j - N_j'$.

When employing the expansion (13) for reconstructing $\tilde{V}$ at each of the points $P(\theta_j, \phi)$, just p unknown outside samples $\tilde{V}(\theta_m)$ are always involved, since the other ones can be reconstructed via (8). Accordingly, by denoting with $\overline{m}$ the index of the last intermediate sample inside the measurement plane on the considered radial line, for each $j = 1,\ldots,J$ we obtain:

$$\tilde{V}\big(\theta_j\big) - \sum_{m=m_0-p+1}^{\overline{m}} \tilde{V}(\theta_m)\, D_M\big(\theta_j - \theta_m\big)\, \Omega_{M''}\big(\theta_j - \theta_m\big) = \\ = \sum_{m=\overline{m}+1}^{\overline{m}+\overline{p}} \tilde{V}(\theta_m) D_M\big(\theta_j - \theta_m\big)\, \Omega_{M''}\big(\theta_j - \theta_m\big) \tag{21}$$

where $\bar{p} \le p$ is the number of external samples to be estimated. These J equations can be rewritten in matrix form as $\underline{\underline{A}}\,\underline{x} = \underline{b}$, where $\underline{b}$ is the sequence of the known terms, $\underline{\underline{A}}$ is a $J \times \bar{p}$ matrix, whose elements $A_{jm} = D_M(\theta_j - \theta_m)\,\Omega_{M''}(\theta_j - \theta_m)$ are given by the weight functions in the considered OSI expansion and $\underline{x}$ is the sequence of the unknown outside samples $\tilde{V}(\theta_m)$, with $m = \overline{m}+1,..., \overline{m}+\bar{p}$. A solution, which is the best approximation in the least squares sense of the linear system (21), can be obtained by using the SVD technique.

Once the outside samples relevant to the considered radial line have been estimated, the voltage values at any point on it can be evaluated via (13).

Note that the matrix $\underline{\underline{A}}$ depends on the samples position on the radial line. In fact, the ρ-coordinate of the regular samples (those obtained as intersection between the radial line and the spiral) increases on increasing the angle ϕ. A Tikhonov regularization approach can be usefully applied [8] to obtain a more accurate solution of the linear system (21). Such a solution corresponds to minimize the functional:

$$\left\| \underline{\underline{A}}\,\underline{x} - \underline{b} \right\|_2^2 + \alpha^2 \left\| \underline{x} \right\|_2^2 \tag{22}$$

α being the regularization parameter. Thus, we can write the regularized solution $\underline{x}_{\text{reg}}$ and the corresponding residual vector $\underline{b} - \underline{\underline{A}}\,\underline{x}_{\text{reg}}$ in term of the SVD of $\underline{\underline{A}}$ in the generic form

$$\underline{x}_{\text{reg}} = \sum_{i=1}^{\bar{p}} f_i \frac{\underline{u}_i^{\text{H}}}{\sigma_i} \underline{v}_i \tag{23}$$

$$\underline{b} - \underline{\underline{A}}\,\underline{x}_{\text{reg}} = \sum_{i=1}^{\bar{p}} (1 - f_i) \underline{u}_i^{\text{H}} \underline{b}\; \underline{u}_i + \sum_{i=\bar{p}+1}^{J} \underline{u}_i^{\text{H}} \underline{b}\; \underline{u}_i \tag{24}$$

In (23) and (24), the symbol H denotes the conjugate transposition operator, σ_i, (i = 1,..., $\bar{p}$) are the singular values of $\underline{\underline{A}}$, ordered from the maximum to the minimum, $f_i = \sigma_i^2 / \left(\sigma_i^2 + \alpha^2\right)$ are the corresponding filter factors, and $\underline{u}_i$, $\underline{v}_i$ are the left and right singular vectors of $\underline{\underline{A}}$, respectively [8]. The choice of the optimal parameter α to be used can be made by means of the L-curve, which is simply a plot of the norm of the regularized solution $\underline{x}_{\text{reg}}$ versus the corresponding residual norm of $\underline{b} - \underline{\underline{A}}\,\underline{x}_{\text{reg}}$ drawn in log-log scale for a set of admissible regularization parameters. In this way, the L-curve displays the compromise between the minimization of these two quantities, which is the heart of any regularization method. With reference to the Tikhonov regularization, the best compromise is represented by the so-called "corner", i.e., the distinct point separating the vertical and the horizontal parts of the curve.

4. NF–FF transformation

The basic theory of probe compensated NF measurements on a plane [7] is based on the application of the Lorentz reciprocity theorem. In the here used reference system, the key relations, for evaluating the FF components E_Θ, E_Φ of the AUT, are:

$$E_\Theta(\Theta,\Phi) = \frac{1}{\Delta}\left(I_H E'_{\Phi_V}(\Theta,-\Phi) - I_V E'_{\Phi_H}(\Theta,-\Phi) \right) \tag{25}$$

$$E_\Phi(\Theta,\Phi) = \frac{1}{\Delta}\left(I_H E'_{\Theta_V}(\Theta,-\Phi) - I_V E'_{\Theta_H}(\Theta,-\Phi) \right) \tag{26}$$

where

$$\Delta = E'_{\Theta_H}(\Theta,-\Phi)\,E'_{\Phi_V}(\Theta,-\Phi) + \\ - E'_{\Theta_V}(\Theta,-\Phi)\,E'_{\Phi_H}(\Theta,-\Phi) \tag{27}$$

$$I_{V,H} = A \cos\Theta\, e^{j\beta d \cos\Theta} \int_{-\infty}^{+\infty}\int_{-\infty}^{+\infty} V_{V,H}(x,y) \cdot \\ \cdot e^{j\beta x \sin\Theta \cos\Phi}\, e^{j\beta y \sin\Theta \sin\Phi}\, dx\, dy \tag{28}$$

A being a constant. Namely, the AUT far field is related to: a) the two-dimensional Fourier transforms I_V and I_H of the voltages V_V and V_H for two independent sets of measurements (the probe is rotated by 90° in the second set); b) the FF components E'_{Θ_V}, E'_{Φ_V} and E'_{Θ_H}, E'_{Φ_H} radiated by the probe and the rotated probe, when used as transmitting antennas. Equations (25) and (26) are valid whenever the probe maintains its orientation with respect to the AUT and this requires that it rotates together with the AUT. Probes exhibiting only a first-order azimuthal dependence in their radiated far field can be used without co-rotation, since V_V and V_H can be evaluated from the measured voltages V_ϕ and V_ρ, via the relations $V_V = V_\phi \cos\phi - V_\rho \sin\phi$, $V_H = V_\phi \sin\phi + V_\rho \cos\phi$.

5. Numerical tests

The reported numerical tests refer to a uniform planar circular array (Fig. 1) having diameter $2a = 30.4\,\lambda$ (λ being the wavelength). Its elements are elementary Huygens sources linearly polarized along the y axis and are radially and azimuthally spaced of $0.95\,\lambda$. An open-ended circular waveguide having radius a' equal to $0.338\,\lambda$ is chosen as probe. The measurement plane is $25\,\lambda$ away from the AUT center and the samples of the probe voltages V_ϕ and V_ρ are collected on a spiral that covers a circular zone of radius $60\,\lambda$. According to the described sampling representation, J = 8 extra rings have been acquired in the peripheral zone. They are spaced at $\Delta\rho = 0.95\lambda$, starting from the end of the measurement circle. It is

worthy to note that, on a given radial line, the number of outside samples is $\bar{p} = 5$. A Tikhonov regularization approach has been applied to obtain the best estimation of the outside samples for all the considered radial lines. We have assumed $p = 17$ in the extrapolation process of the outside samples, whereas $q = 6$ has been adopted both in (8) and in (20) to obtain the involved known samples and the extra data, respectively. Note that the SVD is applied to a small matrix with a negligible computational effort.

Figures 3 and 4 show the amplitude of the output voltage V_V on the radial lines at $\phi = 0°$ and $\phi = 90°$, respectively. They have been reconstructed without using the extrapolation process and putting the outside samples equal to zero. As can be seen in Figs. 5 and 6, by using the proposed estimation procedure, the reconstruction is very accurate not only in the whole measurement region, but also in a zone outside it. It is worthy to note that, in all the cases, $p = 6$ has been adopted when applying (13) for the reconstruction. In order to assess more quantitatively the effectiveness of the proposed approach, the maximum and mean-square reconstruction errors have been evaluated by comparing in the measurement zone the exact voltage values and those reconstructed with and without the estimated outside samples. Figure 7 shows such errors, normalized to the voltage maximum value on the plane, for $\chi = \chi' = 1.20$, and $p = q$ ranging from 2 to 10. As can be seen, the errors evaluated by taking into account the estimated samples decrease until very low levels are reached. On the contrary, those obtained without considering them saturate to constant values, due to the truncation error present near to the boundary of the measurement region. The algorithm stability has been assessed (see Fig. 8) by adding random errors to the exact samples. These errors simulate a background noise, bounded to Δa (dB) in amplitude and with arbitrary phase, and an uncertainty on the data of $\pm\Delta a_r$ (dB) in amplitude and $\pm\Delta\alpha$(degrees) in phase.

The described approach has been applied to recover the plane-rectangular data needed for the NF–FF transformation and lying in a $136\lambda \times 136\lambda$ square grid. Figures 9 and 10 report the AUT pattern in the E-plane, reconstructed via the NF–FF transformation without and with estimated outside samples. As can

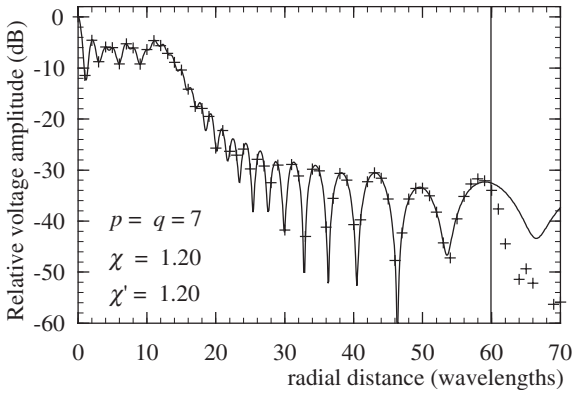

Figure 3 - Amplitude of the probe voltage V_V on the radial line at $\phi = 0°$. Solid line: exact. Crosses: reconstructed without estimated outside samples.

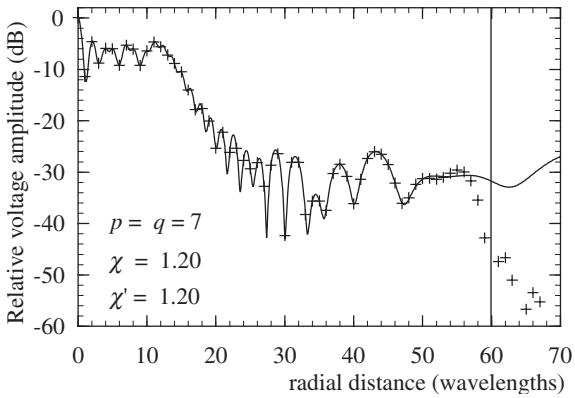

Figure 4 - Amplitude of the probe voltage V_V on the radial line at $\phi = 90°$. Solid line: exact. Crosses: reconstructed without estimated outside samples.

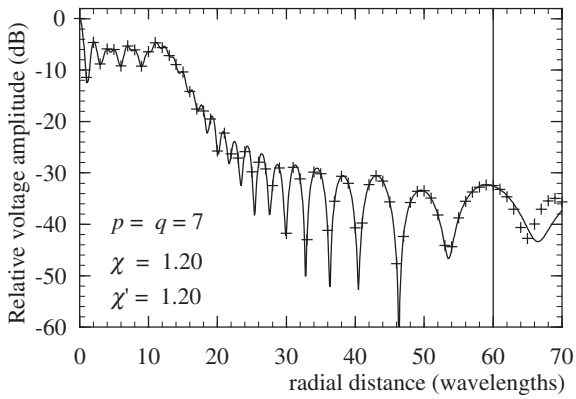

Figure 5 - Amplitude of the probe voltage V_V on the radial line at $\phi = 0°$. Solid line: exact. Crosses: reconstructed with estimated outside samples.

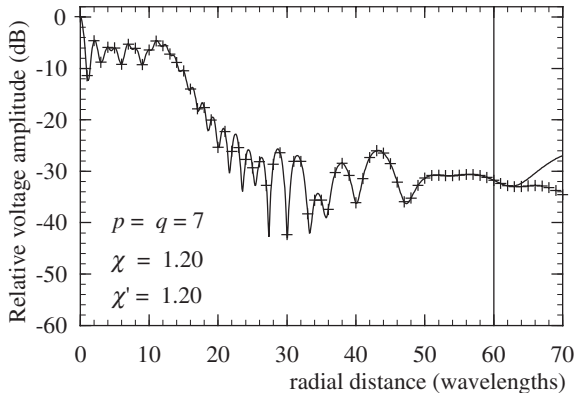

Figure 6 - Amplitude of the probe voltage V_V on the radial line at $\phi = 90°$. Solid line: exact. Crosses: reconstructed with estimated outside samples.

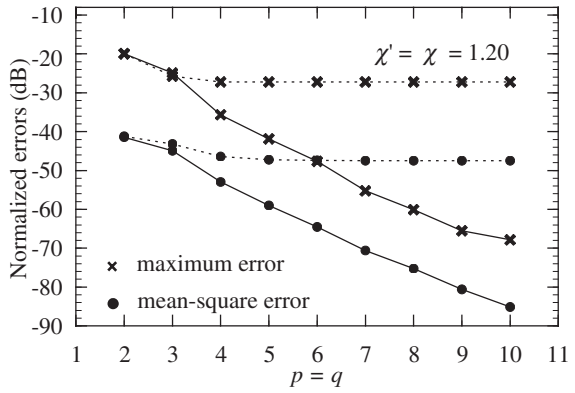

Figure 7 - Normalized reconstruction errors. Dashed lines: without estimated outside samples. Solid lines: with estimated outside samples.

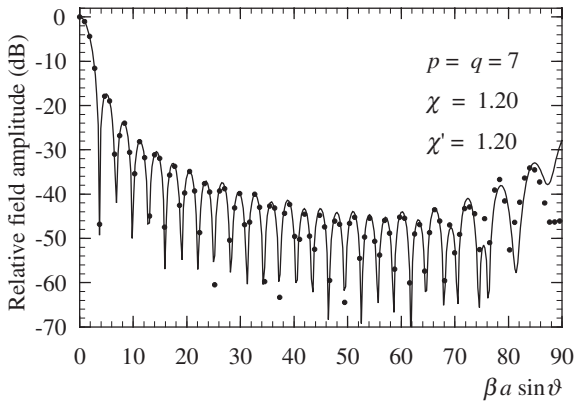

Figure 9 - E-plane pattern. Solid line: exact. Dots: reconstructed via the NF–FF transformation without estimated outside samples.

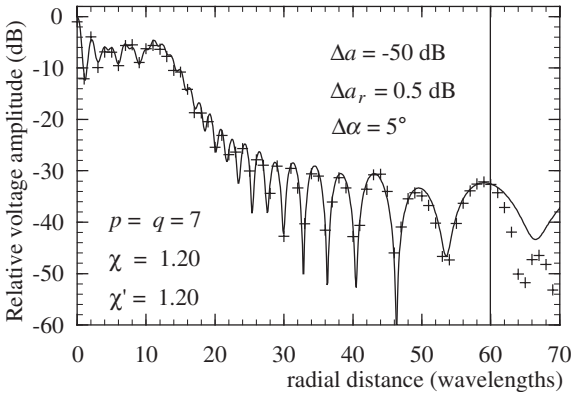

Figure 8 - Amplitude of the probe voltage V_V on the radial line at $\phi = 0°$. Solid line: exact. Crosses: reconstructed with estimated outside samples from error affected data.

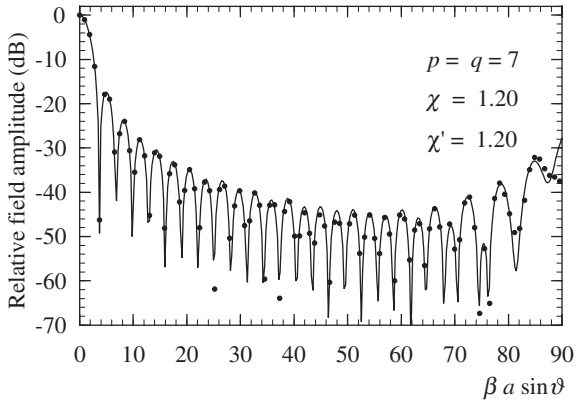

Figure 10 - E-plane pattern. Solid line: exact. Dots: reconstructed via the NF–FF transformation with estimated outside samples.

be seen, the FF reconstruction obtained by considering the estimated samples is accurate in a significantly wider angular range, thus assessing the effectiveness of the technique. Note that the number of employed samples is 10 160. In particular, the number of "extra samples" on the peripheral rings is 2062.

6. REFERENCES

[1] A.D.Yaghjian, "An overview of near-field antenna measurements," *IEEE Trans. Antennas Propagat.*, vol. AP-34, pp. 30-45, 1986.

[2] C.Gennarelli, G.Riccio, F.D'Agostino, and F.Ferrara, *Near-Field – Far-Field Transformation Techniques*, CUES, Salerno, Italy, 2004.

[3] R.G.Yaccarino, L.I.,Williams, and Y.Rahmat-Samii, "Linear spiral sampling for the bipolar planar antenna measurement technique," *IEEE Trans. Antennas Propagat.*, vol. AP-44, pp. 1049-1051, 1996.

[4] F.D'Agostino, C.Gennarelli, G.Riccio, and C.Savarese, "Theoretical foundations of near-field–far-field transformations with spiral scannings, "*Progress in Electromagn. Res.*, *PIER 61,* pp. 193-214, 2006.

[5] O.M.Bucci, F.D'Agostino, C.Gennarelli, G.Riccio, and C.Savarese, "Probe compensated FF reconstruction by NF planar spiral scanning," *IEE Proc. - Microw., Antennas Propagat.,* vol. 149, pp. 119-123, 2002.

[6] O.M.Bucci, C.Gennarelli, and C.Savarese, "Representation of electromagnetic fields over arbitrary surfaces by a finite and nonredundant number of samples," *IEEE Trans. Antennas Propagat.*, vol. 46, pp. 351-359, 1998.

[7] D.T.Paris, W.M.Leach, Jr., and E.B.Joy, "Basic theory of probe-compensated near-field measurements," *IEEE Trans. Antennas Propagat.*, vol. AP-26, pp. 373-379, 1978.

[8] P.C.Hansen, *Rank-deficient and discrete ill-posed peoblems*, SIAM, Philadelphia, 1998.